



Cite this: *Phys. Chem. Chem. Phys.*,  
2020, 22, 3400

# Measuring multiple $^{17}\text{O}$ – $^{13}\text{C}$ $J$ -couplings in naphthalaldehydic acid: a combined solid state NMR and density functional theory approach†‡

Gregory J. Rees,<sup>a</sup> Stephen P. Day,<sup>a</sup> Kristian E. Barnsley,<sup>a</sup> Dinu Iuga,<sup>a</sup>  
Jonathan R. Yates,<sup>b</sup> John D. Wallis<sup>c</sup> and John V. Hanna<sup>\*a</sup>

A combined multinuclear solid state NMR and gauge included projected augmented wave, density functional theory (GIPAW DFT) computational approach is evaluated to determine the four heteronuclear  $^1J(^{13}\text{C},^{17}\text{O})$  couplings in solid  $^{17}\text{O}$  enriched naphthalaldehydic acid. Direct multi-field  $^{17}\text{O}$  magic angle spinning (MAS), triple quantum MAS (3QMAS) and double rotation (DOR) experiments are initially utilised to evaluate the accuracy of the DFT approximations used in the calculation of the isotropic chemical shifts ( $\delta_{\text{iso}}$ ), quadrupole coupling constants ( $C_Q$ ) and asymmetry ( $\eta_Q$ ) parameters. These combined approaches give  $\delta_{\text{iso}}$  values of 313, 200 and 66 ppm for the carbonyl ( $\text{C}=\text{O}$ ), ether ( $-\text{O}-$ ) and hydroxyl ( $-\text{OH}$ ) environments, respectively, with the corresponding measured quadrupole products ( $P_Q$ ) being 8.2, 9.0 and 10.6 MHz. The geometry optimised DFT structure derived using the CASTEP code gives firm agreement with the shifts observed for the ether ( $\delta_{\text{iso}} = 223$ ,  $P_Q = 9.4$  MHz) and hydroxyl ( $\delta_{\text{iso}} = 62$ ,  $P_Q = 10.5$  MHz) environments but the unoptimised experimental XRD structure has better agreement for the carbonyl group ( $\delta_{\text{iso}} = 320$ ,  $P_Q = 8.3$  MHz). The determined  $\delta_{\text{iso}}$  and  $\eta_Q$  values are shown to be consistent with bond lengths closer to 1.222 Å (experimental length) rather than the geometry optimised length of 1.238 Å. The geometry optimised DFT  $^1J(^{13}\text{C},^{17}\text{O})$  coupling to the hydroxyl is calculated as 20 Hz and the couplings to the ether were calculated to be 37 ( $\text{O}-\text{C}=\text{O}$ ) and 32 ( $\text{O}-\text{C}-\text{OH}$ ) Hz. The scalar coupling parameters for the unoptimised experimental carbonyl group predict a  $^1J(^{13}\text{C},^{17}\text{O})$  value of 28 Hz, whilst optimisation gives a value of 27 Hz. These calculated  $^1J(^{13}\text{C},^{17}\text{O})$  couplings, together with estimations of the probability of each O environment being isotopically labelled (determined by electrospray ionisation mass spectrometry) and the measured refocussable transverse dephasing ( $T_2'$ ) behaviour, are combined to simulate the experimental decay behaviour. Good agreement between the measured and calculated decay behaviour is observed.

Received 16th July 2019,  
Accepted 6th January 2020

DOI: 10.1039/c9cp03977e

rscl.li/pccp

## Introduction

In comparison to other prominent organic functionalities, the inception and formation of the C–O bond is a relatively poorly understood process despite its fundamental prominence in many branches of organic, organometallic and industrial chemistry, and chemical engineering.<sup>1</sup> The production of ethers, acetals and ketals, and the initiation of hydrolysis reactions rely intrinsically on the relative strength of the C–O

bond in its particular environment.<sup>2</sup> Some well-established industrial processes are underpinned by the formation of C–O bonds to yield industrial scale commercial products. The Paternò–Büchi reaction is a photochemical process that forms C–O bonds in natural products syntheses, and the Williamson ether synthesis is a widely used industrial process for ether formation.<sup>3,4</sup> Furthermore, hydrogen bonding to the oxygen atom in C–O bonds, (e.g. in esters) can affect their strengths, and may play a role in enzymatic processes pertaining to numerous biological and biomedical applications.<sup>5</sup> More recently, initiatives on biomass utilization have employed homogeneous catalysis for the activation and functionalization of ether C–O sigma ( $\sigma$ ) bonds for F capture and remediation.<sup>6</sup>

The high chemical specificity and ability to probe short range interactions enables solid state NMR to investigate the relationship between a negative O-centred nucleophile and a  $\text{sp}^2$  hybridized electrophilic C centre. In this study solid naphthalaldehydic acid (**1**) and its  $^2\text{H}$ -naphthalaldehydic acid (**2**) counterpart, depicted in

<sup>a</sup> Department of Physics, University of Warwick, Gibbet Hill Road, Coventry, CV4 7AL, UK. E-mail: j.v.hanna@warwick.ac.uk

<sup>b</sup> Department of Materials, Oxford University, 16 Parks Rd, Oxford, OX1 3PH, UK

<sup>c</sup> School of Science and Technology, Nottingham Trent University, Clifton Lane, Nottingham, NG11 8NS, UK

† The experimental data for this study are provided as a supporting dataset from WRAP, the Warwick Research Archive Portal at <http://wrap.warwick.ac.uk/130520>.

‡ Electronic supplementary information (ESI) available. See DOI: 10.1039/c9cp03977e



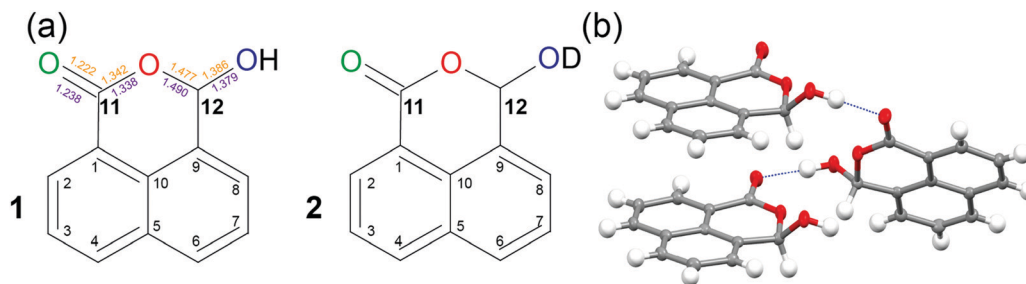


Fig. 1 (a) The structures of the naphthalaldehydic acid variants with the hydroxyl group (1) and the deuterated hydroxyl group (2) as evaluated in this study. The numbering scheme and labels defining the carbonyl ( $\text{C}=\text{O}$ ,  $\text{C}_{11}$ ) and hydroxyl ( $\text{C}-\text{OH}$ ,  $\text{C}_{12}$ ) positions, and the colour scheme denoting the O environments is conserved throughout the manuscript. The experimental (orange) and CASTEP-DFT geometry optimized (purple) bond lengths are also illustrated and summarised in Table 3. (b) The crystal packing scheme of solid naphthalaldehydic acid showing the H-bonding between stacks of molecules related by a twofold screw axis.

Fig. 1(a) and (b), respectively, will be examined using this technique to characterise C–O bonding arrangements with varying strength. This molecule represents a unique structural motif which possesses three O-based functionalities which are in close proximity within the six-membered lactone crown of the naphthalaldehydic structure, thus introducing numerous C–O bonding scenarios. A recent report describes a series of salts in which the lactone ring has opened to produce isolated aldehyde and carboxylate groups, and the  $n-\pi^*$   $\text{C}\cdots\text{O}$  interactions and H-bonding scenarios between them.<sup>7</sup> Some prominent examples of this overall phenomenon included the efficacy and structure–function properties of aspirin,<sup>8</sup> and the stabilisation of chirality in protein and polymer structures.<sup>9–13</sup>

The measurement of scalar (or  $J$ -) couplings between directly bonded or closely proximate NMR active nuclei are routinely exploited to aid molecular structure determination.<sup>14</sup> Scalar coupling values are quantifiable entities emanating from the hyperfine interactions between neighbouring nuclei and is transmitted through the bonding electrons, providing information about connectivity and dynamics between atomic positions.<sup>15</sup> In typical solution state NMR experiments on organic and inorganic compounds, the determination of such couplings can be attained from basic 1D experiments; this is due to fast Brownian motion (on the timescale of the NMR experiment) removing the anisotropic components of all interactions present, thus resulting in high resolution isotropic data. However, it should be emphasised that  $J$ -couplings in solution involving the  $^{17}\text{O}$  nucleus (particularly  $^1J(^{13}\text{C}, ^{17}\text{O})$  couplings) are typically elusive due to the fast quadrupole relaxation of the  $^{17}\text{O}$  nucleus.<sup>16</sup> In contrast, the residual inhomogeneous broadenings commonly experienced in solids usually preclude  $J$  couplings between common nuclei ( $^1\text{H}$ ,  $^{13}\text{C}$ ,  $^{15}\text{N}$ ,  $^{31}\text{P}$ ,  $^{29}\text{Si}$ ,  $^{17}\text{O}$ , etc.) from being measurable in direct observation experiments. Solid state NMR experiments rarely succeed in the achieving the spectral resolution attainable in the solution state because of the existence of higher order cross terms which cannot be completely averaged by MAS, residual dipolar interactions and distributions of isotropic chemical shifts due to structural disorder.<sup>17</sup> However, developments in high speed magic angle spinning (MAS),<sup>18</sup> effective heteronuclear decoupling and pulse sequence development,<sup>19</sup> higher magnetic field strengths, and the GIPAW DFT computation of

NMR parameters<sup>20–23</sup> have all contributed to improved resolution and introduced new rationales for interpreting solid state NMR data. These advances have stimulated a renewed interest in undertaking  $J$ -coupling measurements in the solid state.

The aim of this study is to establish a combined methodology which uses first principles density functional theory (DFT)  $J$ -coupling calculations using the CASTEP code and heteronuclear ( $^{13}\text{C}-^{17}\text{O}$ ) spin echo-based experiments to determine the  $^1J(^{13}\text{C}, ^{17}\text{O})$  couplings within the various C–O moieties of naphthalaldehydic acid which is a complex lactone arrangement with three O-containing functionalities in close proximity. This approach provides a natural complement to single crystal X-ray structure determinations and charge density studies that can collectively interrogate the relative strength of C–O bonds and could be extended to  $\text{C}\cdots\text{O}$  interactions and bond formation scenarios. Solid state NMR  $J$ -coupling measurements are typically achieved using  $J$ -resolved or INADEQUATE experiments, or specific variants of these sequences.<sup>24–29</sup> A key feature of these spin echo-based experiments is that they refocus the evolution of all terms that appear as offsets, including those that are directly induced by chemical shift distributions.<sup>30</sup> This has critical implications for solid state NMR experimentation as the utilisation of these methods allows the indirect detection of  $J$ -couplings, even when inhomogeneous broadenings impede its direct observation and measurement from the more routinely acquired 1D data. As the  $^{17}\text{O}$  nucleus has an extremely low natural abundance (0.037%), there exists a dearth of measured  $^1J(^{13}\text{C}, ^{17}\text{O})$  couplings in both the solid and solution NMR literature. Hung *et al.* demonstrated  $^1J(^{13}\text{C}, ^{17}\text{O})$  measurements from a doubly labelled ( $^{13}\text{C}, ^{17}\text{O}$ ) solid glycine-HCl sample, however no further investigations have been reported from solid systems.<sup>16</sup> This work represents the first study to implement a combined computational and experimental approach to measure multiple  $^1J(^{13}\text{C}, ^{17}\text{O})$  couplings in a more complex organic system to further investigate C–O bond characteristics.

## Experimental section

### Synthesis

Maximum  $^{17}\text{O}$  enrichment of naphthalaldehydic acid **1** with optimal homogeneity was achieved by dissolving the solid (200 mg, 1 mmol) in dioxane (4 ml) whilst stirring under nitrogen,



with 90%  $^{17}\text{O}$  labelled water (Cortecnet, 0.45 ml) being added. Phosphorus pentachloride ( $\sim 2$  mg) was added and the mixture warmed to  $75^\circ\text{C}$  for 24 h. The reaction was cooled, the solvent evaporated *in vacuo*, and the residue left to dry at  $45^\circ\text{C}$  for 1 h. Toluene (18 ml) was added and the mixture heated to reflux, filtered through a warm glass filter funnel, and the filtrate left to crystallise at room temperature to give white crystals (122 mg, 60%), m.p.  $165\text{--}166^\circ\text{C}$ . To test the selectivity of the  $^{17}\text{O}$  enrichment process, a less vigorous process was used where the initial reflux stage was conducted in THF (bp  $66^\circ\text{C}$ ) instead of dioxane (which was heated to  $75^\circ\text{C}$ ), using a reaction time of only 6 h and a lower  $^{17}\text{O}$  concentration of 40% (Cortecnet, 0.45 ml).

The naphthalaldehydic acid (100 mg) was deuterated by dissolving the product in dichloromethane (20 ml), and the filtered solution shaken with  $\text{D}_2\text{O}$  (99%,  $2 \times 2$  ml). The dichloromethane solution was dried with anhydrous sodium sulphate, filtered and evaporated to give the mono-deuterated material.

$^1\text{H}$  NMR (400 MHz,  $(\text{CD}_3)_2\text{CO}$ , 292.1 K):  $\delta$  = 8.36 (1H, dd,  $^3J$  = 7.2, 1.0 Hz, Ar- $H_1$ ), 8.31 (1H, dd,  $^3J$  = 8.4, 1.0 Hz, Ar- $H_1$ ), 8.09 (1H, d,  $^3J$  = 8.2 Hz, Ar- $H_1$ ), 7.71–7.81 (3H, m, Ar- $H_3$ ), 7.20 (1H, d,  $^3J$  = 6.8 Hz, OH), 6.93 (1H, br d,  $^3J$  = 6.0 Hz, CHOH);  $^{13}\text{C}$  NMR (100 MHz,  $(\text{CD}_3)_2\text{CO}$ , 292.1 K):  $\delta$  = 163.6 br (C=O), 134.4, 132.9, 130.8, 129.8, 129.1, 128.0, 127.7, 127.2, 126.1, 121.2 (Ar- $C_{10}$ ), 97.0 br (CHOH).

IR (ATR): 3270 br, 1663, 1623, 1597, 1588, 1516, 1407, 1373, 1356, 1316, 1263, 1248, 1189, 1179, 1109, 1070, 993, 984, 919, 904, 843, 771, 739, 728, 687, 652  $\text{cm}^{-1}$ ; note that the C=O stretch in unlabelled material is  $1675\text{ cm}^{-1}$ .

MS: (LTQ Orbitrap XL, nano-ESI-negative): found: 203.0555 (13), 202.0522 (100), 201.0484 (67), 200.0444 (15), corresponds to *ca.* 6 : 4 : 1 ratio of triply, doubly and singly  $^{17}\text{O}$  labelled naphthalaldehyde anions. Calculated for  $\text{C}_{12}\text{H}_7[^{17}\text{O}]_3$ : 202.0527; for  $\text{C}_{12}\text{H}_7\text{O}_1[^{17}\text{O}]_2$ : 201.0485;  $\text{C}_{12}\text{H}_7\text{O}_2[^{17}\text{O}]$ : 200.0443.

### Solid state NMR

The solid state  $^1\text{H}$  MAS NMR measurement was undertaken at 14.1 T using a Bruker Avance-II+ 600 spectrometer operating at a  $^1\text{H}$  Larmor frequency of 599.4 MHz. The data was acquired using a Bruker 1.3 mm triple resonance probe spinning at 60.0 kHz. A single pulse experiment was implemented using a  $1.25\text{ }\mu\text{s}$  pulse duration (flip angle of  $\pi/4$ ) and a recycle delay of 180 s. This  $^1\text{H}$  MAS NMR data was referenced to the primary standard of tetramethylsilane (TMS,  $\delta_{\text{iso}} = 0$  ppm). A corresponding  $^2\text{H}$  MAS NMR measurement was undertaken at 11.7 T on a Bruker Avance-III 500 spectrometer operating at a  $^2\text{H}$  Larmor frequency of 76.8 MHz. This data was acquired using a 4 mm Bruker MAS double resonance probe operating at a 5 kHz spinning frequency. A single pulse experiment was implemented using a  $1.75\text{ }\mu\text{s}$  pulse duration (flip angle of  $\pi/4$ ) and a recycle delay of 3 s was determined. The  $^2\text{H}$  MAS spectrum was referenced to *d*-chloroform ( $\text{CDCl}_3$ ,  $\delta_{\text{iso}} = 7.26$  ppm) which was compared to the primary reference of TMS- $d_{12}$  ( $\delta_{\text{iso}} = 0$  ppm).<sup>32</sup>

The  $^{13}\text{C}$  MAS NMR data was acquired at 11.7 T using a Bruker Avance-III 500 spectrometer operating at a  $^{13}\text{C}$  Larmor frequency of 125.8 MHz. A  $^1\text{H}$ – $^{13}\text{C}$  cross-polarisation MAS (CPMAS)

experiment was implemented using a Bruker 4 mm double resonance probe which enabled a rotation frequency of 10 kHz. A variable amplitude (70–100%) CPMAS experiment employed an initial  $^1\text{H}$   $\pi/2$  pulse of  $2.5\text{ }\mu\text{s}$ , a contact period of 5 ms, a recycle delay of 600 s and a  $^1\text{H}$  decoupling field of  $\sim 100$  kHz during acquisition. The  $^{13}\text{C}$  CPMAS NMR data was referenced to the primary standard of tetramethylsilane (TMS,  $\delta_{\text{iso}} = 0$  ppm) *via* a secondary solid alanine reference ( $\delta_{\text{iso}}(\text{CH}_3) = 20.5$  ppm,  $\delta_{\text{iso}}(\text{CH}) = 50.5$  ppm and  $\delta_{\text{iso}}(\text{COOH}) = 177.8$  ppm). The measurement of the  $^1J(^{13}\text{C}, ^{17}\text{O})$  coupling constants were performed using a modified spin-echo experiment as previously described by Hung *et al.*<sup>16</sup> A  $^1\text{H}$ – $^{13}\text{C}$  CP preparation of magnetisation (see above) was followed by a refocussing  $\pi$  pulse (CP- $\tau$ - $\pi$ - $\tau$ ) on both the  $^{13}\text{C}$  and  $^{17}\text{O}$  channels thus forming an echo. The  $^{13}\text{C}$  and  $^{17}\text{O}$   $\pi$  pulse duration on each channel was  $6\text{ }\mu\text{s}$ . The  $\tau$  delays were incremented from 0 to 15 ms, with 100 kHz of  $^1\text{H}$  decoupling applied throughout. The 2D  $^1\text{H}$ – $^{13}\text{C}$  Lee–Goldberg heteronuclear correlation experiment used the same cross polarisation preparation as described above and implemented homonuclear Lee–Goldberg  $^1\text{H}$ – $^1\text{H}$  decoupling during acquisition. No additional resolution enhancement in the  $^1\text{H}$  spectrum was observed with the implementation of homonuclear decoupling.

For the quadrupolar  $^{17}\text{O}$  ( $I = 5/2$ ) nucleus MAS NMR studies were performed at 14.1, 16.5 and 20.0 T using Bruker Avance-II+ 600, Bruker Avance-III HD 700 and Bruker Avance-III 850 instruments operating at  $^{17}\text{O}$  Larmor frequencies of 81.3, 94.9 and 115.2 MHz, respectively. A Bruker 3.2 mm double resonance probe was used at each field which facilitated a MAS frequency of 20.0 kHz for each measurement. All  $^{17}\text{O}$  MAS NMR data were acquired using a rotor-synchronised Hahn echo experiment ( $\theta$ - $\tau$ - $2\theta$ - $\tau$ -acquire). A ‘non-selective’ (solution)  $\pi/2$  pulse time of  $3\text{ }\mu\text{s}$  was calibrated using 10%  $\text{H}_2^{17}\text{O}$  which represented a ‘selective’  $\pi/2$  (solid) pulse of  $1\text{ }\mu\text{s}$ ; a  $\theta = \pi/2 = 1\text{ }\mu\text{s}/2\theta = \pi = 2\text{ }\mu\text{s}$  combination was used for all measurements. A recycle delay of 5 s was used throughout; this was carefully checked against acquisitions using recycle delays of up to 60 s. All  $^{17}\text{O}$  apparent shifts (centre-of-gravity,  $\delta_{\text{cg}}$ ) and isotropic chemical shifts ( $\delta_{\text{iso}}$ ) are reported against a primary reference of  $\text{H}_2^{17}\text{O}$  ( $\delta_{\text{iso}} = 0$  ppm).<sup>32</sup> Additional  $^{17}\text{O}$  double rotation (DOR) experiments using odd order sideband suppression<sup>33</sup> were undertaken at 9.4, 11.7 and 14.1 T using Bruker Avance-III HD 400, Bruker Avance-III 500 and Bruker Avance-II+ 600 spectrometers operating at the  $^{17}\text{O}$  Larmor frequencies of 54.1, 67.8 and 81.3 MHz, respectively. The measurements at each field were performed using Samoson designed DOR probes which functioned with external rotor spinning frequencies of 1.3–1.9 kHz and internal rotor spinning frequencies of 5.9–9.7 kHz.

All central transition spectra from the  $^{17}\text{O}$  MAS NMR data of **1** acquired at 14.1, 16.5 and 20.0 T were simulated using the DMFit<sup>34</sup> simulation package to determine the experimental isotropic chemical shift ( $\delta_{\text{iso}}$ ) and quadrupole ( $C_Q$ ,  $\eta_Q$ ) NMR parameters (see Table 1 and Fig. 3(a), (c) and (e), respectively). The CASTEP calculated NMR parameters for  $\delta_{\text{iso}}$ ,  $^1J_{\text{OC}}$ ,  $C_Q$  and  $\eta_Q$  (see Tables 2 and 3) were used as input into the SIMPSON



**Table 1** The  $^{17}\text{O}$  NMR parameters of naphthalaldehydic acid **1** obtained from the deconvolution of the  $^{17}\text{O}$  MAS NMR data shown in Fig. 3 compared with those parameters elucidated from the  $^{17}\text{O}$  DOR NMR of the  $^{17}\text{O}$  enriched molecule **1** and the  $^{17}\text{O}/^2\text{H}$  enriched molecule **2** as presented in Fig. 5

Site	<sup>17</sup> O MAS NMR						<sup>17</sup> O DOR NMR				<sup>17</sup> O( <sup>2</sup> H) DOR NMR				
	$\delta_{\text{iso}}^{a/}$	$C_Q^{e/}$	$C_Q^{b/}$	$\eta_Q^c$	$\eta_Q^b$	$P_Q^{d/}$	$P_Q^{d/}$	$\delta_{\text{cg}}^{d/}$	$\delta_{\text{cg}}^{/}$	$P_Q^{d/}$	$P_Q^{/}$	$\delta_{\text{cg}}^{d/}$	$\delta_{\text{cg}}^{/}$	$P_Q^{d/}$	$P_Q^{/}$
	ppm	MHz	MHz			MHz	MHz			MHz	ppm			ppm	MHz
			Error		Error				Error		Error		Error		Error
C=O	313	8.2	0.1	0.03	0.02	8.2	0.1	285	19	7.3	1.7	308	2	8.1	0.1
–O–	200	8.9	0.1	0.25	0.01	9.0	0.1	173	20	8.2	1.5	199	1	9.0	0.1
–OH/–OD	66	9.6	0.4	0.81	0.08	10.6	0.4	63	19	10.4	0.1	16	32	8.6	2.5

<sup>a</sup> IUPAC isotropic shift convention averaged from the multiple field simulations:  $\delta_{\text{iso}} = (\delta_{11} + \delta_{22} + \delta_{33})/3$ . <sup>b</sup> Error derived from average of deconvolutions at three magnetic fields. <sup>c</sup> EFG tensor conventions:  $|V_{33}| \geq |V_{22}| \geq |V_{11}|$ ,  $C_Q = e^2qQ/h$ ,  $\eta_Q = (V_{11} - V_{22})/V_{33}$  ( $1 \geq \eta_Q \geq 0$ ). <sup>d</sup> Quadrupole parameter:  $\delta_{\text{cg}} (\text{ppm}) = \delta_{\text{iso}} - (3/500) (P_Q^2/\nu_0^2) \times 10^6$  and  $P_Q (\text{MHz}) = C_Q (1 + \eta_Q^2/3)^{1/2}$ .

**Table 2** The first principles GIPAW DFT (CASTEP) calculated  $^{17}\text{O}$  NMR parameters produced using the XRD derived (experimental) and geometry optimised (GO) versions of the naphthalaldehydic acid **1** crystal structure. The DFT determined shifts are calibrated using  $\delta_{\text{iso}} = -[\sigma - \sigma_{\text{ref}}]$ , where  $\sigma_{\text{ref}} = 262 \text{ ppm}^{20}$

O site	GIPAW DFT calculated $^{17}\text{O}$ NMR parameters (experimental (XRD) structure)				GIPAW DFT calculated $^{17}\text{O}$ NMR parameters (geometry optimised structure)			
	$\delta_{\text{iso}}/\text{ppm}$	$C_Q/\text{MHz}$	$\eta_Q$	$P_Q/\text{MHz}$	$\delta_{\text{iso}}/\text{ppm}$	$C_Q/\text{MHz}$	$\eta_Q$	$P_Q/\text{MHz}$
C=O	320	8.3	0.09	8.3	307	8.1	0.31	8.2
-O-	210	9.3	0.30	9.4	223	9.3	0.25	9.4
-OH/-OD	26	9.7	0.65	10.4	62	9.5	0.82	10.5

**Table 3** The  $^1J(^{13}\text{C}, ^{17}\text{O})$  coupling constants between the  $C_{11}$  and  $C_{12}$  positions and the  $^{17}\text{O}$  labelled C=O, -O- and -OH oxo functionalities as determined by GIPAW DFT calculations using the CASTEP code from the geometry optimised and experimental versions of the naphthalaldehydic acid structure **1**. These calculated  $^1J(^{13}\text{C}, ^{17}\text{O})$  coupling constants are compared to experiment via the dephasing behaviour shown in Fig. 6 which was measured using a heteronuclear spin echo experimental technique

Coupling constant	$^{13}\text{C}$ nuclei	$^{17}\text{O}$ nuclei	Bond length/ $\text{\AA}$	Bond angle/ $^\circ$ O-C-O	$^1J_{\text{co}}/\text{Hz}$	Optimised bond length/ $\text{\AA}$	Optimised bond angle/ $^\circ$ O-C-O	Optimised $^1J_{\text{co}}/\text{Hz}$
$^1J_{\text{CO1}}$	$C_{11}$	C=O	1.222	117.5	28	1.238	117.4	32
$^1J_{\text{CO2}}$		-O-	1.342	117.5	37	1.338	117.4	37
$^1J_{\text{CO3}}$	$C_{12}$	-O-	1.477	106.7	32	1.490	107.4	32
$^1J_{\text{CO4}}$		-OH	1.386	106.7	21	1.379	107.4	20

4.2.1<sup>35</sup> simulation package to generate a direct comparison between experimental and calculated data. The SIMPSON input files are given in Table S3 (ESI<sup>†</sup>).

### First principle DFT geometry optimisation and magnetic resonance calculations

All density functional theory (DFT) calculations were performed using the CASTEP 16.1<sup>21</sup> code which employs Kohn-Sham DFT methodology using periodic plane-waves under the ultrasoft pseudopotential approximation. The generalized gradient approximation for the exchange correlation energy was employed using the Perdew-Burke-Ernzerhof solids functional (PBE-sol). Pseudopotentials were generated 'on-the-fly' using the standard Accelrys Software Materials Studio pseudo-atom definitions. Each calculation was converged with respect to basis-set size and Brillouin zone  $k$  point sampling to at least an accuracy of 0.4 mH ( $\sim 0.000002\%$  of total energy) per atom for each of the systems under investigation. To confirm this level of energy convergence was sufficient to produce accurate ionic forces, energy minimisation with respect to ionic positions was repeated with increasing plane wave cut off energy and density of  $k$  points within the Monkhorst-Pack Brillouin zone grid.

This level of convergence was achieved using a plane wave cut-off energy of 900 eV for system, and by invoking  $k$  point Monkhorst-Pack grids of  $3 \times 2 \times 2$ .

Geometry optimisation and H position optimisation calculations were performed on all systems using the over-converged values described previously to ensure accurate forces. For these structural optimisations, the lattice parameters were kept fixed whilst the atomic positions were optimised to a force tolerance of  $0.05 \text{ eV } \text{\AA}^{-1}$ , a maximum ionic displacement of  $1 \times 10^{-3} \text{ \AA}$  and a total energy change of  $2 \times 10^{-5} \text{ eV}$  per atom. NMR parameter calculation of the chemical shift,<sup>22,36</sup> electric field gradient tensors<sup>20</sup> and  $J$ -couplings<sup>23,37</sup> invoked the gauge included projector augmented wave (GIPAW) DFT method which extended the pseudopotential (valence electron approximation) approximation to recover all electron charge densities. This approach demonstrated that the NMR parameters depend more sensitively upon the electron density than the total energy, so each NMR parameter will be more sensitive to basis set truncation errors than to total energies. This is compensated for by the over-convergence of the basis set to a level which experience suggests will produce fully converged NMR parameters. Consequently, these calculations were completed





using the plane wave cut-off and  $k$ -point Monkhorst–Pack grids described earlier.

In order to calculate isotropic chemical shifts for the  $^{17}\text{O}$  nucleus the relationship  $\delta_{\text{iso}} = -[\sigma - \sigma_{\text{ref}}]$  was employed, where  $\sigma$  is the calculated isotropic shielding calculated against a bare atom, and  $\sigma_{\text{ref}}$  is the previously determined reference isotropic shielding of 262 ppm when compared against a bare atom.<sup>38</sup> These calculations used the same basis set convergence (0.4 mH) as the original calculations to minimise the propagation of errors.

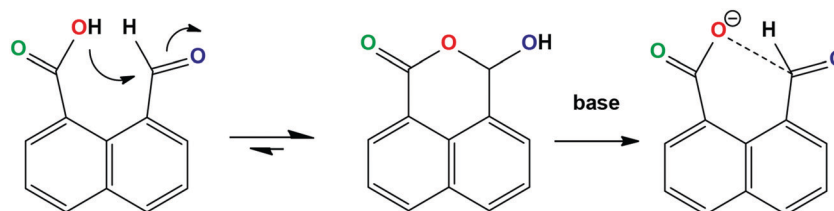
## Results and discussion

The homogenous  $^{17}\text{O}$  enrichment of solid naphthalaldehydic acid **1** was achieved by heating to 75 °C in 90%  $^{17}\text{O}$  labelled water under acid catalytic conditions in hot dioxane for 24 h, with the resulting product recrystallized from toluene. The electrospray ionisation mass spectrometry (ESI-MS) of the resultant anion suggested that it was characterised by a ratio of triply labelled: doubly labelled: mono labelled molecules of  $\sim 6:4:1$ . A recently reported single crystal X-ray structure determination of **1** shows that the head group is essentially a closed lactone ring arrangement supporting the three proximate O positions referred to as carbonyl (C=O), ether (–O–) and hydroxyl (–OH) groups for the purpose of the remaining discussion. However, open ring configurations can be realised when molecule **1** is deprotonated to give salts with various cations which exhibit interactions between the negatively charged carboxylate ( $\text{CO}_2^-$ ) anion and the aldehyde ( $\text{CH=O}$ ) functionality (see Scheme 1 below).<sup>7</sup>

As observed in Fig. 1(b), the crystalline salt naphthalaldehydic acid **1** has a cyclic lactone structure with only one crystallographically unique molecule comprising the asymmetric unit of the crystal. There exists intermolecular H-bonding between the C=O functionality and the –OH moiety on an adjacent molecule constrained by a twofold screw axis, with the two symmetry related H-bonds associated with each molecule assuming an  $\text{O}\cdots\text{O}$  distance of 2.754(4) Å.<sup>7</sup> There is an anomeric interaction between the two O atoms attached to the methine C leading to a short C–OH bond length of 1.387 Å and a long C–O(C=O) bond length of 1.477 Å due to donation of lone pair electron density from the hydroxyl O atom into the adjacent methine  $\text{CH–O(C=O)}$  bond.<sup>7</sup> In comparison, a typical unperturbed C–O bond length is usually observed to fall between these values at  $\sim 1.43$  Å.<sup>39</sup>

The  $^1\text{H}$  MAS NMR data from naphthalaldehydic acid measured at 14.1 T under fast MAS conditions ( $\nu_r = 60$  kHz) is shown in Fig. 2(a). This spectrum shows a single broad resonance with no individual proton environments able to be resolved from this signal, despite the acquisition of this data under high field and fast MAS conditions. The aromatic, hydroxyl and methine  $^1\text{H}$  species are all expected to appear at similar isotropic chemical shifts ( $\delta$  6.8–8.4 ppm in solution), and the strong homogeneous  $^1\text{H}$ – $^1\text{H}$  dipolar interaction broadens all resonances thus resulting in a single unresolved feature. It is possible that both the  $^1\text{H}$  and  $^{13}\text{C}$  resonances suffer from anisotropic bulk magnetic susceptibility (ABMS) broadening, however this broadening typically only increases the linewidth by  $\sim 1$  ppm.<sup>40</sup> These problems are commonly observed in highly complex aromatic systems and heavy (but not complete) deuteration of the sample is required to significantly increase spectral resolution.<sup>41</sup>

The  $^{17}\text{O}$  labelled naphthalaldehydic acid sample **1** was selectively deuterated at the hydroxy position to form a doubly  $^{17}\text{O}/^2\text{H}$  enriched variant **2** (see Fig. 1(a)) to investigate (and reduce) the potential of  $^1\text{H}$  motional modulation effects on the  $^{17}\text{O}$  MAS and DOR NMR data (*vide infra*). The  $^2\text{H}$  MAS NMR data from this quadrupolar ( $I = 1$ ) nucleus shown in Fig. 2(b) depicts a broad satellite transition spectrum with a  $^2\text{H}$  quadrupole coupling constant ( $C_Q$ ) of  $\sim 200$  kHz being measured from the simulation of this data. Previous measurements of  $^2\text{H}$   $C_Q$  values from various enriched –OD arrangements demonstrate that  $C_Q$  occurs within the range of  $\sim 190$ – $290$  kHz;<sup>42,43</sup> the  $C_Q$  characterising the –OD moiety in this hydroxyl–lactone species represents a value at the low end of this range thus suggesting that partial motional averaging of this interaction is evident. This value is significantly smaller than the predicted  $C_Q$  value of  $\sim 308$  kHz as computed using the CASTEP code (see Table S1 in the ESI†). These DFT calculations in their basic form do not account for rotation, vibration or libration of the –OD bond, hence any subsequent motional averaging of the static quadrupole interaction is not modelled. Recently, it has been suggested that deuteration can also reduce the point symmetry of the moiety.<sup>44</sup> It is important to note that the  $\delta_{\text{iso}}(^2\text{H})$  for the –OD species is  $\sim 8.0$  ppm, and this is corroborated by the 1D  $^1\text{H}$  MAS and 2D  $^1\text{H}$ – $^{13}\text{C}$  HETCOR MAS NMR data depicted in Fig. 2(a) and (d). The 2D  $^1\text{H}$ – $^{13}\text{C}$  HETCOR data of Fig. 2(d) clearly shows that all protonated C species are correlated with the broad  $^1\text{H}$  resonance at  $\sim 8.0$  ppm, indicating that the  $\delta_{\text{iso}}(^1\text{H})$  value is not resolved from the more intense  $^1\text{H}$  resonances associated with the aromatic protons. Collectively, the observations of a more deshielded  $^1\text{H}$  chemical shift ( $\delta_{\text{iso}}(^1\text{H}) \sim 8.9$  ppm) and a



Scheme 1



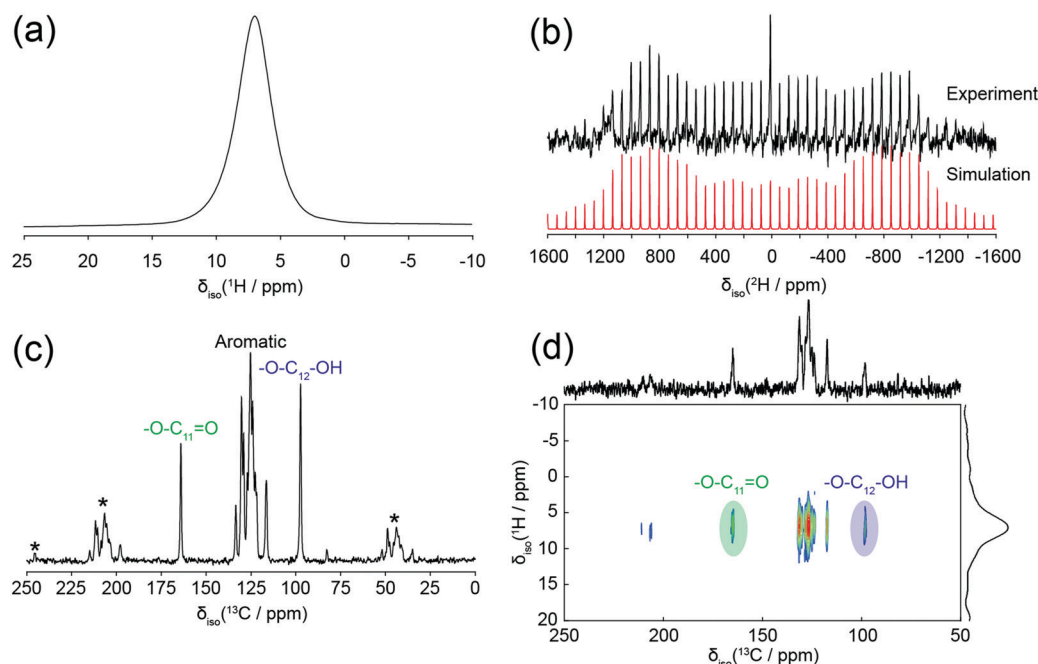


Fig. 2 The characterisation of solid naphthalaldehydic acid **1** using (a)  $^1\text{H}$  MAS NMR ( $\nu_0 = 599.4$  MHz,  $\nu_r = 60$  kHz), (b)  $^2\text{H}$  MAS NMR ( $\nu_0 = 76.8$  MHz,  $\nu_r = 5$  kHz) with experimental data (black) and simulation (red), (c)  $^{13}\text{C}$  CPMAS (5 ms contact time) NMR ( $\nu_0 = 125.8$  MHz,  $\nu_r = 10$  kHz) with the carbonyl, aromatic and alcohol regions labelled, and (d) a 2D  $^1\text{H}$ – $^{13}\text{C}$  Lee–Goldberg heteronuclear correlation experiment (5 ms contact time) which utilised homonuclear  $^1\text{H}$  decoupling throughout the evolution and acquisition periods. The asterisks (\*) in the  $^{13}\text{C}$  CPMAS NMR data in (c) denote the presence of spinning sidebands.

partial motional averaging of the  $^2\text{H}$  quadrupole interaction ( $C_Q \sim 200$  kHz) indicates that the bond covalence characterising the  $-\text{OH}$  group is of intermediate strength, while the intermolecular H-bonding interaction inherent to the crystal structure of **1** (influencing the  $-\text{OH}$  proton) is weak.<sup>31,38</sup>

Solid state  $^{17}\text{O}$  MAS NMR data from **1** measured at 20.0 T ( $\nu_0 = 115.2$  MHz), 16.5 T ( $\nu_0 = 94.9$  MHz) and 14.1 T ( $\nu_0 = 81.3$  MHz) presented in Fig. 3(a)–(c), respectively, shows the three O species present in the six membered hydroxyl-lactone ring form of the naphthalaldehydic acid lactone crown are all influenced by substantial second order quadrupole interactions. The highly characteristic second order broadened quadrupole resonances are fully resolved at 20.0 T, however due to the  $1/B_0$  dependence of the quadrupole interaction the observed linewidths increase with decreasing  $B_0$ , consequently reducing the resolution of the lower field data. Corresponding 2D  $^{17}\text{O}$  3QMAS data from **1** acquired at 16.5 T shown in Fig. 4 clearly demonstrates the chemical purity of this system, and that very high structural order is reflected by the absence of any distributions in the chemical shift and/or distributions of quadrupole NMR parameters. Previous studies have established that H-bond motion can modulate the multiple quantum excitation and evolution processes in the MQMAS experiment thus inducing detrimental effects on the resolution observed in the F1 dimension, however this is also not observed here.<sup>38</sup>

Simulation of the  $^{17}\text{O}$  1D data for the  $\text{C}=\text{O}$  species (*i.e.* the most deshielded  $^{17}\text{O}$  environment) yields an isotropic chemical shift of  $\delta_{\text{iso}} = 313$  ppm and quadrupole parameters of  $C_Q = 8.2$  MHz/ $\eta_Q = 0.03$ . A  $^{17}\text{O}$   $\delta_{\text{iso}}$  value of this magnitude is low compared to a ketone

group, but it is within the reported limits of typical carboxylic acid and lactone functionalities.<sup>46,47</sup> Conversely, the observed  $^{17}\text{O}$  resonance from the hydroxyl ( $-\text{OH}$ ) species is the most shielded ( $\delta_{\text{iso}} = 66$  ppm) and represents a larger quadrupole interaction with  $C_Q = 9.6$  MHz/ $\eta_Q = 0.81$ . Both sets of  $^{17}\text{O}$  quadrupole parameters measured for both the  $\text{C}=\text{O}$  and the  $-\text{OH}$  groups are in firm agreement with previously reported data in the literature observed for amino acid-HCl salts.<sup>38,46,48</sup> The high  $\eta_Q$  value for the  $-\text{OH}$  species, and corresponding low  $\eta_Q$  value for the  $\text{C}=\text{O}$  species are typical for  $^{17}\text{O}$  nuclei bonded to larger conjugated aromatic moieties.<sup>38,49</sup> In previous studies on amino acids, it has been reported that the  $^{17}\text{O}$  asymmetry parameter ( $\eta_Q$ ) is close to zero for  $\text{C}\cdots\text{O}$  distances in a  $\text{C}=\text{O}$  functionality of  $\sim 1.22$  Å, while it appears to increase rapidly for longer bond lengths. Simulation of the  $^{17}\text{O}$  resonance from the ether ( $-\text{O}-$ ) linkage (located between the  $\text{C}=\text{O}$  and  $-\text{OH}$  resonances) in this lactone structure yields an isotropic chemical shift of  $\delta_{\text{iso}} = 200$  ppm and quadrupole parameters of  $C_Q = 8.9$  MHz/ $\eta_Q = 0.25$ . All isotropic chemical shift and quadrupole parameters characterising the three O species comprising this lactone structure are in agreement with previously reported values for the lactone of 2-[1,2,3- $^{17}\text{O}_3$ ]acetylbenzoic acid which is the only other reported labelled lactone structure studied by solid state NMR.<sup>47</sup> Despite the use of high magnetic fields in this study, no chemical shift anisotropy (CSA) contributions were required to facilitate the accurate simulation the data in Fig. 3(a)–(c), suggesting that CSA influences are small in comparison to the dominant quadrupole interaction and subsequently eliminated by MAS.



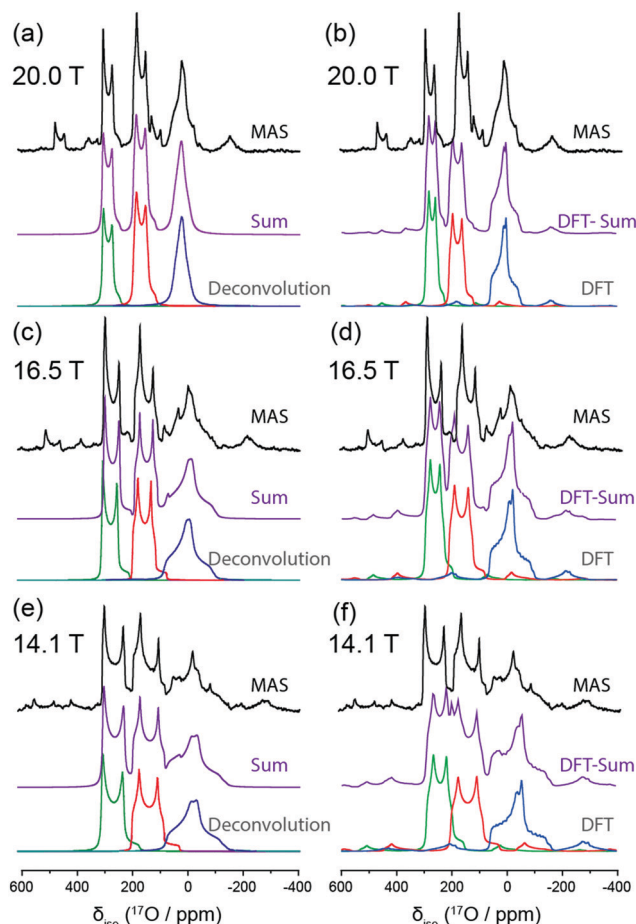


Fig. 3 The  $^{17}\text{O}$  MAS NMR data and spectral deconvolution from  $^{17}\text{O}$  enriched naphthalaldehydic acid **1** acquired at (a) 20.0 T ( $\nu_0 = 115.2$  MHz,  $\nu_r = 20$  kHz), (c) 16.5 T ( $\nu_0 = 94.9$  MHz,  $\nu_r = 20$  kHz), (e) 14.1 T ( $\nu_0 = 81.3$  MHz,  $\nu_r = 20$  kHz), compared against their corresponding SIMPSON<sup>45</sup> simulations (b), (d), (f) generated using GIPAW DFT calculations of the NMR parameters from the single crystal naphthalaldehydic acid **1** structure using the CASTEP code. In each case, the green resonance represents the carbonyl (C=O) species, the red resonance represents the ether (–O–) species, the blue resonance represents the hydroxyl group (–OH), and the spectral sum shown in purple.

For moderate-weak H-bonded systems, a previously established empirical relationship between the  $^{17}\text{O}$  quadrupole coupling constant of the O species involved in X–H $\cdots$ O (X = N, O) H bonds and the X $\cdots$ O distance across the whole X–H $\cdots$ OH bond takes the form:<sup>46,50,51</sup>

$$C_Q \approx 1.5199(R(\text{X}\cdots\text{O})) + 3.9987 \quad (1)$$

In molecule **1**, the distance between two O atoms (–C–OH $\cdots$ O=C–) bridging the H bond is 2.787 Å. Upon substitution of this O $\cdots$ O distance into eqn (1) a predicted  $C_Q$  value of 8.23 MHz is obtained which compares very favourably with the measured  $C_Q$  of 8.2 MHz as reported in Table 1, thus supporting moderate-weak H bond character in the structure of **1**.

In addition, there is a strong correlation between the C=O bond length and the carbonyl  $^{17}\text{O}$  isotropic chemical shift ( $\sim 1200$  ppm Å<sup>–1</sup>), with a shift of  $\sim 313$  ppm representing a

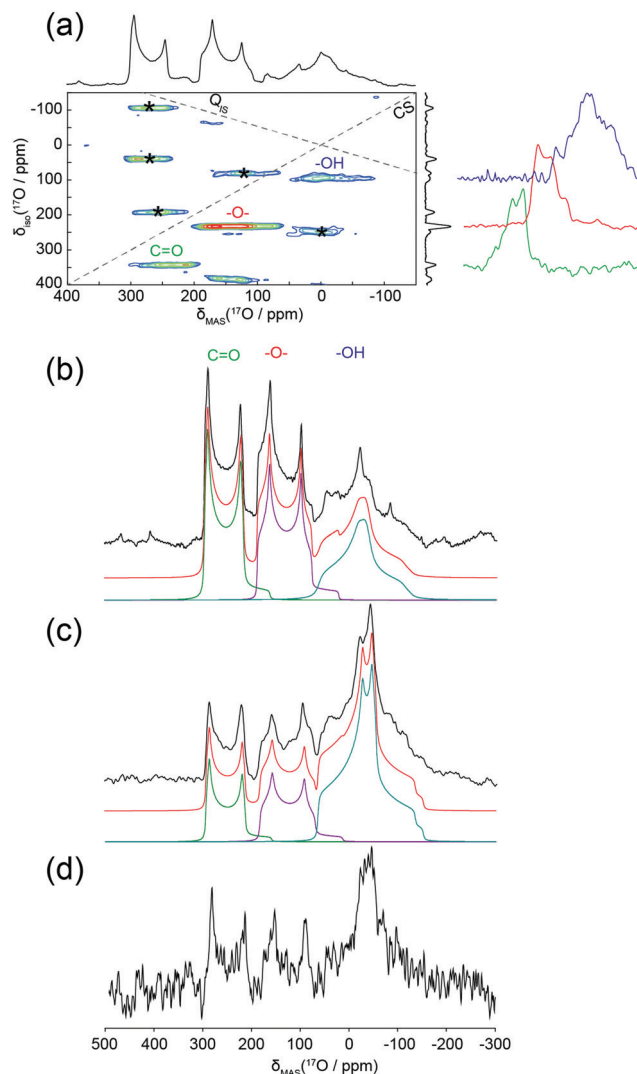


Fig. 4 The (a) 2D  $^{17}\text{O}$  3QMAS NMR data of naphthalaldehydic acid **1** (16.5 T,  $\nu_r = 20$  kHz), the individual 1D projections from 400 to  $-150$  ppm are given along the F1 axis and the spinning sidebands are represented with asterisks (\*), shown with 1D  $^{17}\text{O}$  MAS NMR data (14.1 T,  $\nu_r = 20$  kHz) for (a) a homogeneously and optimally enriched sample of **1** using 90% labelled  $\text{H}_2\text{O}$  showing a  $\sim 1:1:1$  intensity distribution (refluxed in dioxane, 75 °C, 24 h), (b) an inhomogeneously and less enriched sample of **1** using 40% labelled  $\text{H}_2\text{O}$  showing a  $\sim 1:1:2$  intensity distribution (refluxed in THF, 66 °C, 6 h), and a doubly labelled  $^2\text{H}/^{17}\text{O}$  enriched sample **2** where the  $^2\text{H}$  enrichment is performed after the initial  $^{17}\text{O}$  labelling using the 90%  $\text{H}_2\text{O}$  precursor (refluxed in dioxane, 75 °C, 24 h). Note the marked loss of  $^{17}\text{O}$  signal intensity in (d) compared to (b) upon further reaction required to achieve the  $^2\text{D}$  enrichment post the  $^{17}\text{O}$  enrichment, hence no 3QMAS data was achieved from the  $^2\text{H}$ -naphthalaldehydic acid **2** sample.

bond length of 1.222 Å.<sup>48</sup> A comparison of the C=O bond lengths to C= $^{17}\text{O}$   $\delta_{\text{iso}}$  values compiled by Pike *et al.*,<sup>22</sup> together with the GIPAW DFT data reported by Gervias *et al.*,<sup>52</sup> produces an overall empirical correlation relating the  $^{17}\text{O}$   $\delta_{\text{iso}}$  value to the carbonyl bond length ( $R(\text{C}=\text{O})$ ):

$$\delta_{\text{iso}}(\text{C}=\text{O}) \approx 1751 - 1177(R(\text{C}=\text{O})) \quad (2)$$

The C=O bond length of **1** measured in the single crystal X-ray structure determination at 100 K is 1.222 Å, and the DFT



geometry optimisation yields a longer C=O bond length of 1.238 Å. From Table 3, the measured  $^{17}\text{O}$   $\delta_{\text{iso}}$  value of the C=O value is 313 ppm (from MAS NMR); when this value is introduced to eqn (2) a bond length of 1.223 Å is predicted, suggesting the room temperature NMR measurements are in firm agreement with the single crystal X-ray structure determination (performed at 100 K) despite the large temperature difference between the two measurements. Correspondingly, as the MAS NMR measured  $^{17}\text{O}$   $\eta_{\text{Q}}$  value of the carbonyl is close to zero, then it can be presumed that the bond length is closer to the unoptimized 1.222 Å, as any C=O bond length significantly above 1.2 Å gives a  $\eta_{\text{Q}} > 0$  value.<sup>53</sup> Support for the crystallographic derived structure by highly accurate  $^{17}\text{O}$  solid state NMR measurements is necessary to gauge the temperature variations between the NMR (298 K) and crystallographic (100 K) measurements. These observations infer that accurate calculated  $^1J(^{13}\text{C}, ^{17}\text{O})$  couplings can be obtained from DFT-CASTEP calculations (notionally undertaken at 0 K) on high quality crystal structure data.

From inspection of the spectral and computationally generated data exhibited in Fig. 3 and Tables 1 and 2, there exists a very strong correlation between the directly measured and simulated  $^{17}\text{O}$  MAS NMR data (see Fig. 3(a), (c) and (e), and Table 1) and the GIPAW DFT calculated  $^{17}\text{O}$  NMR interaction parameters from a geometry optimised structure of **1** using the CASTEP code (see Fig. 3(b), (d) and (f) and Table 2). In particular, the experimentally determined –OH data ( $\delta_{\text{iso}} = 66$  ppm,  $C_{\text{Q}} = 9.6$  MHz,  $\eta_{\text{Q}} = 0.81$ ), –O– data ( $\delta_{\text{iso}} = 200$ ,  $C_{\text{Q}} = 8.9$ ,  $\eta_{\text{Q}} = 0.25$ ) and C=O data ( $\delta_{\text{iso}} = 313$  ppm,  $C_{\text{Q}} = 8.2$  MHz and  $\eta_{\text{Q}} = 0.03$ ) show an excellent agreement with the corresponding DFT results (–OH,  $\delta_{\text{iso}} = 62$  ppm,  $C_{\text{Q}} = 9.5$  MHz,  $\eta_{\text{Q}} = 0.85$ ; –O–,  $\delta_{\text{iso}} = 223$  ppm,  $C_{\text{Q}} = 9.3$  MHz,  $\eta_{\text{Q}} = 0.25$ ; C=O,  $\delta_{\text{iso}} = 307$  ppm,  $C_{\text{Q}} = 8.1$  MHz and  $\eta_{\text{Q}} = 0.31$ ) when geometry optimisation is implemented. These correlations are marginally stronger than those derived from calculations using non-geometry optimised structures; this is particularly evident when comparing the MAS NMR measured and DFT calculated –OH  $\delta_{\text{iso}}$  values when geometry optimisation is omitted. In this case, a discrepancy of ~40 ppm exists. Nevertheless, the strength of the above correlations suggests that the GIPAW DFT method represents a very sound approximation for describing the electronic configuration of O species in organic solids, and this approach thus presents a solid foundation on which to underpin  $^1J(^{13}\text{C}, ^{17}\text{O})$  coupling calculations in the naphthalaldehydic acid system **1**. The DFT calculations also highlight that both geometry optimised and direct calculations on the X-ray derived structure need to be considered when calculating the  $^1J(^{13}\text{C}, ^{17}\text{O})$  couplings in this system.

Unlike the conventional MAS NMR technique, the Double Rotation (DOR) experiment involves spinning the sample about two angles to enable averaging of both the  $P_2$  and  $P_4$  terms of the 4th order Legendre polynomial, which describes the angular dependences of the second order quadrupole interaction. The first order quadrupole broadening is reduced by sample rotation around the familiar magic angle of  $54.7^\circ$  with respect to  $B_0$ , while the second order quadrupole broadening is eliminated by simultaneous rotation at  $54.7^\circ$  and a second angle of  $30.6^\circ$  with

respect to the magic angle. The two major advantages that the DOR NMR technique offers are, (a) the observed (featureless) centre-of-gravity shift ( $\delta_{\text{cg}}$ ) yields greater resolution than conventional MQMAS experiments which are limited by the number of attainable slices defining the F1 dimension, and (b) the DOR experiment uses a single pulse excitation experiment in comparison to two-pulse or three-pulse MQMAS experiments which possess limited pulse efficiencies. The greater resolution and superior signal-to-noise ratio afforded by the DOR technique is met with technical challenges; sample rotation at two angles simultaneously is difficult to stabilise, and the limited rotational rates achievable by the inner and outer rotors introduces large residual spinning sideband manifolds which necessitate acquisitions at multiple spinning rates to isolate the central transition.<sup>33,54</sup>

For a quadrupolar nucleus such as  $^{17}\text{O}$ , the apparent centre-of-gravity shift ( $\delta_{\text{cg}}$ ) is comprised of both field independent isotropic chemical shift ( $\delta_{\text{iso}}$ ) and field dependent second-order quadrupole shift ( $\delta_{\text{Q,iso}}^{(2)}$ ) components:

$$\delta_{\text{cg}} = \delta_{\text{iso}} + \delta_{\text{Q,iso}}^{(2)}(I, m) \quad (3)$$

where

$$\delta_{\text{Q,iso}}^{(2)}(I, m) = (3C_{\text{Q}}^2 / (40\nu_0^2 T^2 (2I - 1)^2)) [I(I + 1) - 9m(m - 1) - 3] (1 + \eta_{\text{Q}}^2 / 3) \quad (4)$$

For the central transition of an  $I = 5/2$  nucleus such as  $^{17}\text{O}$ , eqn (4) reduces to:

$$\delta_{\text{cg}}(\text{ppm}) = \delta_{\text{iso}}(\text{ppm}) - (3/500)(P_{\text{Q}}^2 / \nu_0^2) \times 10^6 \quad (5)$$

where  $\nu_0$  is the  $^{17}\text{O}$  Larmor frequency and  $P_{\text{Q}}$  is the quadrupole product (related to the quadrupole coupling constant,  $C_{\text{Q}}$ ), which is defined by:

$$P_{\text{Q}} = C_{\text{Q}} \sqrt{(1 + \eta_{\text{Q}}^2 / 3)} \quad (6)$$

Hence, for featureless data that precludes simulation of the central transition spectrum to ascertain the characteristic NMR parameters, this approach enables variable  $B_0$  field data to be analysed graphically *via* the linear relationship of eqn (5), thus allowing  $\delta_{\text{iso}}$  to be determined from the y-intercept and  $P_{\text{Q}}$  to be elucidated from the slope.<sup>55–59</sup>

High resolution data afforded by the  $^{17}\text{O}$  DOR technique allows some subtle aspects of motion affecting the O positions to be detected. The characterisation of these properties is an important prerequisite to the measurement and calculation of  $^1J_{\text{CO}}$  couplings. Table 1 summarises the  $\delta_{\text{iso}}$  and  $P_{\text{Q}}$  data elucidated from the variable field (14.1, 11.7 and 9.4 T)  $^{17}\text{O}$  DOR measurements and the graphical approach outlined above for **1** (see Fig. 5(a)–(d)) and **2** (see Fig. 5(e)–(h)). Each spectrum shows the centre-of-gravity shifts ( $\delta_{\text{cg}}$ ) identified; these were isolated from the spinning sideband manifolds by varying the spinning frequency of the outer rotor over a range of 1.3–1.9 kHz. From the undeuterated system **1** the determined  $^{17}\text{O}$   $\delta_{\text{iso}}$  values for the carbonyl (C=O), ether (–O–) and hydroxyl (–OH) species are 285, 173 and 63 ppm, respectively, while the analogous  $\delta_{\text{iso}}$  values of 308, 199 and 16 ppm are obtained





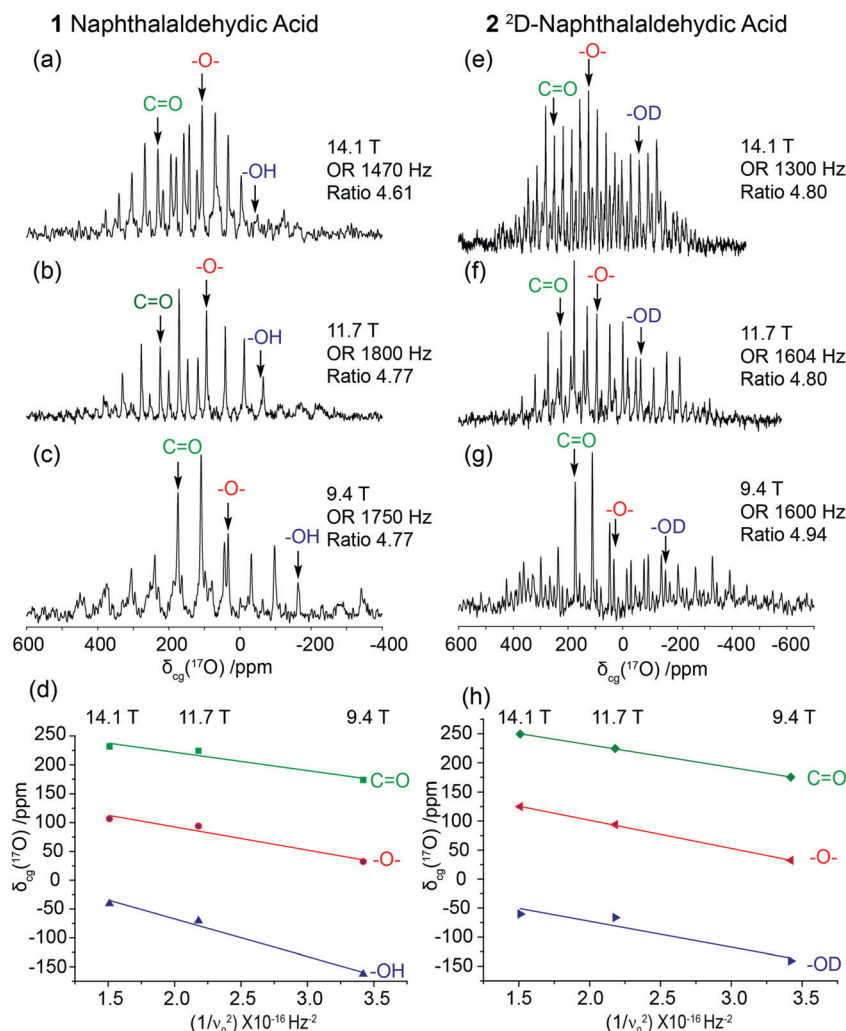


**Fig. 5** The solid state  $^{17}\text{O}$  DOR spectra of naphthalaldehydic acid at (a and e) 14.1 T ( $\nu_0 = 81.3$  MHz), (b and f) 11.7 T ( $\nu_0 = 67.8$  MHz) and (c and g) 9.4 T ( $\nu_0 = 54.1$  MHz). The resonances for C=O, -O- and -OH are labelled in each case and are determined by spinning the samples at a minimum of three different frequencies. Results from undeuterated naphthalaldehydic acid **1** are given in a, b and c, and results from deuterated naphthalaldehydic acid **2** are given in e, f and g. The outer rotor frequencies are denoted as 'OR', and the inner:outer rotor frequency ratios are labelled 'ratio'. From plots of centre-of-gravity ( $\delta_{\text{cg}}$ ) for each DOR resonance against  $1/\nu_0^2$  (d, h),  $\delta_{\text{cg}}$  is observed to be field (or  $\nu_0$ ) dependent through second order quadrupole effects from the spin  $I = 5/2$   $^{17}\text{O}$  nucleus such that  $\delta_{\text{cg}} (\text{ppm}) = \delta_{\text{iso}} (\text{ppm}) - (3/500 \times P_Q^2/\nu_0^2) \times 10^6$ , thus permitting graphical estimates for  $\delta_{\text{iso}}$  (y intercept) and  $P_Q$  (slope) for molecules **1** and **2**.

from the deuterated version **2**. Upon deuteration, a marked deshielding of  $\sim 23$ – $26$  ppm in the  $^{17}\text{O}$   $\delta_{\text{iso}}$  values are observed for the C=O and -O- moieties, which is in contrast with the increased shielding of  $\sim 47$  ppm observed for the -OH species.

Previous studies have demonstrated that the deuteration of protonated oxo functionalities in solid organic systems improves the resolution obtained in the  $^{17}\text{O}$  DOR experiment. This is achieved by damping the heteronuclear dipolar proton coupling which homogeneously broadens the  $^{17}\text{O}$  resonance.<sup>60–63</sup> This is corroborated by the data in Fig. 5 where the  $^{17}\text{O}$  resonance for the -OD (see Fig. 5(e)–(h) for **2**) moiety is significantly narrower and of greater intensity than its -OH counterpart (see Fig. 5(a)–(d) for **1**), especially at the higher fields of 11.7 and 14.1 T. As observed from Table 1 and Fig. 5(d) and (h), the data for the C=O and -O- moieties from the undeuterated sample **1** show an inferior overall correlation on the linear regression and

greater errors on each individual measurement in comparison to their counterparts from the deuterated sample **2**. This is a consequence of the broader  $^{17}\text{O}$  resonances due to proton motion in the H-bond which induces additional cooperative modes of motion throughout the other O functionalities. Furthermore, for the C=O and -O- moieties the measured  $\delta_{\text{iso}}$  and  $P_Q$  values from the DOR experiment closely corroborate those reported from the MAS, MQMAS and geometry optimised DFT (GO-DFT) data. In comparison, for both samples **1** and **2** the overall correlations described in the linear regression for the -OH species are inferior to those described above for the C=O and -O- moieties. As suggested above, a reduced correlation for the -OH data (sample **1**) is expected to emanate from proton heteronuclear dipolar coupling in the H-bonded arrangement; however, the -OD data (sample **2**) exhibits a more reduced correlation and much larger errors. This contradicts previously



reported evidence that proposes sample deuteration reduces these errors, promoting more resolved  $^{17}\text{O}$  DOR data, and enables more accurate measurements of the  $\delta_{\text{iso}}$  and  $P_Q$  parameters.<sup>33</sup> This anomaly suggests that the reduced correlations/larger errors from 2 originate from lower point energy of the OD bond and results in an isotope effect on the NMR parameters.<sup>62,63</sup> The deuteration procedure of  $^{17}\text{O}$  enriched sample 1 (using  $\text{D}_2\text{O}$ ) to produce sample 2 does not yield a homogeneous doubly labelled  $^2\text{D}/^{17}\text{O}$  system. Some proportion of the original  $^{17}\text{O}$  enrichment has exchanged with  $^{16}\text{O}$  producing a complex mixture of  $^2\text{D}/^{17}\text{O}$ ,  $^2\text{D}/^{16}\text{O}$ ,  $^1\text{H}/^{17}\text{O}$  and  $^1\text{H}/^{16}\text{O}$  species, thus producing a complex distribution of isotope effects. This phenomenon is demonstrated in Fig. 4(d) where  $^{17}\text{O}$  MAS NMR data from the deuterated sample 2 (which originated as sample 1) exhibits greatly inferior signal/noise in comparison to sample 1 shown in Fig. 4(b). These complex isotope affects clearly directly influence upon the  $^{17}\text{O}$   $\delta_{\text{iso}}$  and  $P_Q$  parameters characterising each O environment, and the deuteration of molecule 1 can produce measured NMR parameters which are not directly comparable to those calculated from the single crystal derived structure. The process of deuteration of hydroxyl environments to reduce heteronuclear dipolar coupling, and potentially reduce the point symmetry of the moiety, is occasionally employed in the literature. Here, we show this is not best employed when trying to accurately compare diffraction derived DFT NMR parameters and the experimental MAS data. Overall, the GIPAW DFT-derived  $C_Q$  and  $\eta_Q$  parameters show a strong correlation with the MAS and MQMAS achieved parameters, therefore for the following  $^1J$  determinations the experimentally determined parameters will be used.

The spin echo dephasing data from the (undeuterated) naphthalaldehydic acid system 1 is presented in Fig. 6, and the measured heteronuclear  $^1J(^{13}\text{C}, ^{17}\text{O})$  coupling constants are summarised in Table 3. This study represents only the second measurement of  $^1J(^{13}\text{C}, ^{17}\text{O})$  coupling constants in the solid state. While the first was demonstrated on a doubly  $^{13}\text{C}/^{17}\text{O}$  labelled solid glycine-HCl sample,<sup>16</sup> this work focusses on a uniformly labelled  $^{17}\text{O}$  system which possesses multiple O positions which are in close proximity.

A CT-selective  $^{17}\text{O}$   $\pi$ -pulse in a heteronuclear spin echo experiment only refocuses the central-transition (CT) spin states, consequently confining the dephasing behaviour of the  $^{13}\text{C}$  signals observed in Fig. 6 to only those  $^{13}\text{C}$  spins bonded to  $^{17}\text{O}$  spins in the  $+1/2$  or  $-1/2$  CT spin states. Presuming 100%  $^{17}\text{O}$  enrichment of an isolated  $^{13}\text{C}$ - $^{17}\text{O}$  two spin system, only 1/3 of  $^{13}\text{C}$  spins attached to  $^{17}\text{O}$  CT ( $+1/2$  or  $-1/2$ ) spin states will show a cosine  $J$ -modulation, while the other 2/3 of the  $^{13}\text{C}$  spins will show no cosine modulation as they couple to the satellite transition (ST)  $+5/2$ ,  $+3/2$ ,  $-3/2$  or  $-5/2$  spin states. Hence, a  $J$ -resolved experiment utilising a CT-selective  $^{17}\text{O}$  pulse for a  $^{13}\text{C}$ - $^{17}\text{O}$  spin pair will exhibit a cosine modulation (presuming no  $T_2'$  contribution) that goes from an initial signal intensity of 1, down to a minimum signal of  $S(\tau)_{\text{het}} = 0.33$ , with a 0.66 signal intensity for a  $J$ -evolution time of  $^{1/2}J$ . However, the relatively broad nature ( $\sim 41$  kHz) of the multiple  $^{17}\text{O}$  environments in naphthalaldehydic acid means uniformly exciting the three oxygen environments required non-selective pulses, therefore accurate SIMPSON simulations are required to evaluate the data with respect to the pulse lengths used, and fitting the decay using a function is challenging.

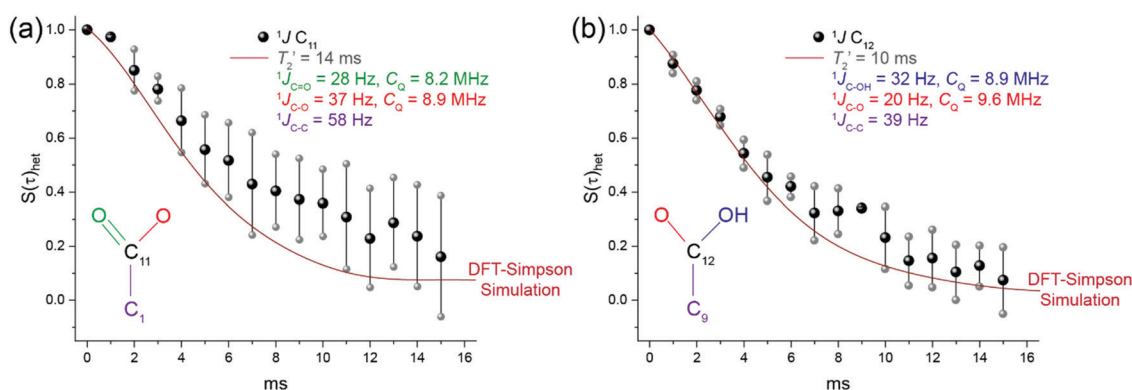


**Fig. 6** The experimental (black) and DFT predicted (red, SIMPSON simulated)  $^{13}\text{C}/^{17}\text{O}$  heteronuclear spin echo dephasing behaviour for (a)  $\text{C}_{11}$  and (b)  $\text{C}_{12}$  acquired at 11.7 T ( $\nu_r = 11$  kHz) as a function of evolution time  $\tau$  (0 to 16 ms). The predicted  $^{13}\text{C}/^{17}\text{O}$  heteronuclear spin echo dephasing behaviour (red line) is derived using GIPAW DFT (CASTEP) calculations of the one-bond dominant  $^1J(^{13}\text{C}, ^{17}\text{O})$  and  $^1J(^{13}\text{C}, ^{13}\text{C})$  coupling constants ( $^1J_{\text{C}11=\text{O}}$ ,  $^1J_{\text{C}11-\text{O}}$ ,  $^1J_{\text{C}11-\text{C}1}$ ,  $^1J_{\text{C}12-\text{O}2}$ ,  $^1J_{\text{C}12-\text{O}1}$  and  $^1J_{\text{C}12-\text{C}9}$ ) and simulated using the SIMPSON 4.2.1 package. The contributions from  $nJ$ -couplings ( $n > 2$ ) are predicted by CASTEP to be minimal and are therefore ignored. The experimental quadrupole coupling constants, which are in good agreement with the DFT results, are used throughout. As SIMPSON does not consider  $T_2'$ , then these were measured using a simple homonuclear spin-echo. The experimental and predicted behaviour  $S(\tau)_{\text{het}} = 0$  ms is normalised to an intensity of 1. The individual compositions, derived from experimental quadrupole parameters, CASTEP  $^1J$  couplings and numerical SIMPSON simulations are deconvoluted in Fig. S1 and S2 (ESI $^\ddagger$ ), up to 32 ms, the results were multiplied with the  $T_2'$  results and their enrichment probabilities:  $p_{\text{O}1\text{O}2} = p_{\text{O}3\text{O}4} = 80\%$ ; probabilities that  $\text{C}_{11}$  or  $\text{C}_{12}$  is directly bonded to two enriched  $^{17}\text{O}$  species,  $p_{\text{O}1} = p_{\text{O}2} = p_{\text{O}3} = p_{\text{O}4} = 7.5\%$ ; probabilities that  $\text{C}_{11}$  or  $\text{C}_{12}$  is directly bonded to one enriched  $^{17}\text{O}$  species,  $p_{\text{none}} = 5\%$ ; probability that  $\text{C}_{11}$  or  $\text{C}_{12}$  are not directly bonded to any enriched  $^{17}\text{O}$  species. Therefore,  $\text{C}_{11} = 0.85 \times \text{SIMPSON output of } ^1J_{\text{C}11=\text{O}}, ^1J_{\text{C}11-\text{O}}, 0.075 \times ^1J_{\text{C}11-\text{O}}, 0.075 \times ^1J_{\text{C}11-\text{O}}, 1.1\%$  (natural abundance  $^{13}\text{C}$ )  $\times ^1J_{\text{C}11-\text{C}1}$ , all multiplied by a  $T_2'$  of 14 ms. An example of the SIMPSON input file is given in the ESI $^\ddagger$ , Table S3. As the natural abundance of the  $^{13}\text{C}$  isotope is 1.1%, these species will induce minor contributions to the dephasing curve and therefore these were considered in the DFT derived SIMPSON simulations.



All data presented in Fig. 6 were acquired using a modified spin echo sequence as detailed by Hung *et al.*,<sup>16</sup> with the simulation of each multi-component spin echo dephasing curve being achieved using SIMPSON.<sup>45</sup> Analytical expressions for deriving isolated  $^1J$ -couplings have been developed by Duma *et al.*, with the quadrupolar contributions to the scalar coupling explored by Perras and Bryce.<sup>64,65</sup> SIMPSON 4.2.1 cannot simulate multiple  $^1J$ -couplings with multiple quadrupole coupling constants. Therefore, the simulation was broken up into their individual one-bond components and multiplied together. The  $\pi$  pulse length (6  $\mu$ s, 41 kHz), was also considered in the SIMPSON calculation to account for any errors or issues caused by finite pulse lengths, this pulse length was chosen as it is the same as the linewidth of the three oxygen environments.

The output of the SIMPSON simulations were then scaled to represent the oxygen enrichment, which was determined by high-resolution ESI-MS. This gave the following probabilities,  $p$ :

$p_{O1O2} = p_{O3O4} = 80\%$ ; probabilities that  $C_{11}$  or  $C_{12}$  is directly bonded to two enriched  $^{17}\text{O}$  species,

$p_{O1} = p_{O2} = p_{O3} = p_{O4} = 7.5\%$ ; probabilities that  $C_{11}$  or  $C_{12}$  is directly bonded to one enriched  $^{17}\text{O}$  species,

$p_{\text{none}} = 5\%$ ; probability that  $C_{11}$  or  $C_{12}$  are not directly bonded to any enriched  $^{17}\text{O}$  species.

As the mass spectrometry analyses cannot differentiate the absolute ratios of the enriched  $\text{O}_1$  ( $C_{11}=\text{O}$ ),  $\text{O}_2$  ( $C_{11}-^{17}\text{O}$ ),  $\text{O}_3$  ( $-^{17}\text{O}-C_{12}$ ) or  $\text{O}_4$  ( $C_{12}-^{17}\text{OH}$ ) species within **1**, it is assumed that their contributions are equal. This assumption is supported by the  $\sim 1:1:1$  ratio of the three O environments in the multiple field  $^{17}\text{O}$  MAS and MQMAS NMR data represented in Fig. 3, 4(a) and (b). It should be noted that the overnight refluxing method (dioxane, 75  $^\circ\text{C}$ , 24 h) for  $^{17}\text{O}$  enrichment (see Fig. 3 and 4(b)) provides a uniformly labelled product for **1** which is thus preferred for this study, in comparison to the labelled product derived from shorter and milder (THF, 66  $^\circ\text{C}$ , 6 h) reaction conditions (see Fig. 4(c)) which highlights a preferential  $^{17}\text{O}$  enrichment of the  $-\text{OH}$  position. The DFT derived SIMPSON outputs do not consider the transverse relaxation contribution to the decays, therefore  $T_{2C11}'$  and  $T_{2C12}'$  were measured using a homonuclear spin echo sequence and upon these the  $^1J(^{13}\text{C}, ^{17}\text{O})$  coupling modulation is superimposed. These times are estimated by conventional homonuclear  $^{13}\text{C}$  spin echo ( $\pi/2-\tau-\pi-\tau$ -acquire) measurements to be  $14 \pm 2$  ms and  $10 \pm 4$  ms for the  $C_{11}$  and  $C_{12}$  positions, respectively.

The GIPAW DFT calculated  $^1J(^{13}\text{C}, ^{17}\text{O})$  coupling constants for the O positions are derived from the single crystal structure determination of **1**,<sup>7</sup> with these calculations being performed on both the geometry optimised and the experimental structures, coupled with associated dispersion corrections. These results are summarised in Table 3. Key to the effectiveness of this computational approach for these  $^1J(^{13}\text{C}, ^{17}\text{O})$  coupling constants is the highly accurate characterisation of **1** involving the more routinely GIPAW DFT calculated NMR parameters

such as  $\delta_{\text{iso}}$ ,  $C_Q$  and  $\eta_Q$  as presented in Fig. 3, and Tables 1 and 2, which demonstrates that the ultrasoft 'on-the-fly' O pseudo-potential is particularly optimised for  $^{17}\text{O}$  NMR measurements in organic solids. This provides the simulation of the dephasing characteristics for  $C_{11}$  and  $C_{12}$  shown in Fig. 6(a) and (b) using the calculated  $^1J(^{13}\text{C}, ^{17}\text{O})$  coupling constants ( $^1J_{CO1}$ ,  $^1J_{CO2}$ ,  $^1J_{CO3}$  and  $^1J_{CO4}$ ) with greater statistical importance.

As the  $C_{11}$  and  $C_{12}$  positions are not  $^{13}\text{C}$  labelled, the spin echo intensities at larger evolution times are difficult to determine, as they cannot be accurately discriminated from the noise. The error in each data point grows cumulatively for increasingly longer evolution times; as observed from Fig. 6, these dephasing measurements were truncated at a maximum evolution time of 15 ms. The contributions from neighbouring proton species are removed by high power  $^1\text{H}$  (100 kHz) decoupling during the evolution and acquisition periods; however, the  $^XJ$  couplings to neighbouring  $^{13}\text{C}$  spins are not suppressed. The  $^1J$ -coupling from  $C_{11}$  to  $C_1$  and  $C_{12}$  to  $C_9$  are 58 and 39 Hz, respectively. As the natural abundance of the  $^{13}\text{C}$  isotope is 1.1%, these species will induce minor contributions to the dephasing curve and therefore these were considered in the DFT derived SIMPSON simulations. Extended homonuclear  $^1J(^{13}\text{C}, ^{13}\text{C})$  contributions are predicted by CASTEP to have an insignificant contribution to the decay (Table S2, ESI $^\ddagger$ ), and as there is no  $^{13}\text{C}$  labelling in the structure, the maximum contribution of this  $^1J(^{13}\text{C}, ^{13}\text{C})$  coupling is 1.1% of  $\cos(\pi J_{CC}\tau)$  to the overall result, these may account for a minor source of error in the observed decay. Using high power decoupling limits the acquisition times you can safely record the data, therefore the cosine modulation feature which is predicted at a  $\tau$  between 20 to 24 ms was not possible to observe. This would also be challenging to reproduce accurately due to reduced signal-to-noise at these larger  $\tau$  delays and the need for high power decoupling at these extreme lengths is likely to cause damage to the probe.

Despite these sources of error, the results presented in Fig. 6 suggest that overall methodology invoked above appears to be a robust approach for calculating multiple  $^1J(^{13}\text{C}, ^{17}\text{O})$  couplings in a complex arrangement containing multiple oxo functionalities in the solid state. In particular, it is evident that GIPAW DFT calculations of  $^1J(^{13}\text{C}, ^{17}\text{O})$  coupling constants are accurate as observed by the strong correlation between the experimental dephasing behaviour and the simulated  $S(\tau)_{\text{het}}$  behaviour (adopting the isolated spin system approximations above) using calculated values of  $^1J_{CO1}$ ,  $^1J_{CO2}$ ,  $^1J_{CO3}$  and  $^1J_{CO4}$  from CASTEP. The correlation between the calculated data using the proposed model and the experimental data is excellent for the three nuclear spin system involving  $C_{12}$  which is directly bonded to the methine ( $-\text{O}-$ ) and hydroxyl ( $-\text{OH}$ ) moieties (*i.e.*  $^1J_{CO3}$  and  $^1J_{CO4}$ ). It should be noted that the reduced correlation describing  $C_{11}$  involves  $^1J_{CO1}$  coupling to the  $\text{C}=\text{O}$  moiety which is influenced by intramolecular H-bonding to the  $-\text{OH}$  species in an adjacent molecule. Furthermore, the errors in the  $C_{11}$  heteronuclear spin echo experiment were larger, due to insufficient signal to noise, possibly due to less efficient cross polarisation.

It is interesting to note that the magnitudes of the two  $^1J(^{13}\text{C}, ^{17}\text{O})$  couplings to the central ether  $-\text{O}-$  linkage reflect the corresponding bond lengths involved. The  $^1J(^{13}\text{C}, ^{17}\text{O})$  coupling



constant for the shorter bond length C=O species is 37 Hz (carbonyl C–O bond length: 1.338 Å), which is larger than the coupling constant of 32 Hz to the more distant CH–OH (methine C–O bond length: 1.490 Å). In contrast, the  $^1J(^{13}\text{C}, ^{17}\text{O})$  coupling constant between the methine C and the –OH species is smaller than that to the ether –O– atom (20 Hz *cf.* 32 Hz) despite having a significantly shorter bond length (1.379 Å *cf.* 1.490 Å). As mentioned above, –OH motion within the weak H-bonding arrangement can modulate and diminish the magnitude of this  $^1J(^{13}\text{C}, ^{17}\text{O})$  coupling, however the bond angle disposition as proposed by the Karplus relationship may also contribute to this marked reversal in this trend.<sup>15,66</sup> Although calculations<sup>67</sup> and measurements<sup>68</sup> of  $^1J(^{13}\text{C}, ^{17}\text{O})$  coupling constants characterising the CO and CO<sub>2</sub> gas phase systems have been reported (measured/calculated; 16.4/17.2 Hz and 16.1/17.1 Hz, respectively), the only existing measurement of  $^1J(^{13}\text{C}, ^{17}\text{O})$  couplings ascertained from a real solid state system pertains to glycine-HCl where  $^1J(\text{C}=\text{O}) = 25$  Hz and  $^1J(\text{C}-\text{OH}) = 28$  Hz.<sup>16</sup> The determined  $^1J(^{13}\text{C}, ^{17}\text{O})$  coupling constants that characterise solid naphthalaldehydic acid **1** summarised in Table 3 are comparable to these previous values, and this study reports the first  $^1J(^{13}\text{C}, ^{17}\text{O})$  measurements on ether –O– linkages. This work has demonstrated that measurements of  $^1J(^{13}\text{C}, ^{17}\text{O})$  coupling constants is not limited to selectively labelled highly isolated spin systems in small molecules, and that this information can be elucidated from larger and more complex spin systems which are isotopically enriched by more routine synthetic methods.

## Conclusions

A combined  $^{17}\text{O}$  MAS, 3QMAS and DOR NMR approach has been utilised to accurately characterise the O positions in naphthalaldehydic acid **1** and to assess the accuracy of the first principles GIPAW DFT calculations for deriving the associated  $^{17}\text{O}$  NMR parameters. The initial phase of this study demonstrated that  $^{17}\text{O}$  NMR parameters such as the isotropic chemical shift ( $\delta_{\text{iso}}$ ) and quadrupole parameters ( $C_Q$ ,  $\eta_Q$ ) were well correlated with those emanating from the GIPAW DFT calculations using the CASTEP code. Heteronuclear  $^1J(^{13}\text{C}, ^{17}\text{O})$  measurements were undertaken on this system which possesses multiple O functionalities in the hydroxy lactone head group of the molecule. These measurements represent the first assessment of multiple  $^1J(^{13}\text{C}, ^{17}\text{O})$  couplings from a single molecule in the solid state, and they were also evaluated against the scalar coupling calculations resulting from first principles GIPAW DFT calculations and SIMPSON simulations. For the modified spin-echo dephasing experiment focussing on the C<sub>11</sub> and C<sub>12</sub> positions in **1**, the dephasing of the magnetisation in each case relates to two three-spin ( $^{17}\text{O}-^{13}\text{C}-^{17}\text{O}$ ) systems in which the O positions are enriched. This experiment cannot isolate the individual  $^1J(^{13}\text{C}, ^{17}\text{O})$  contributions and a weighted average dephasing curve is produced which can only be deconvoluted by simulation using  $^1J(^{13}\text{C}, ^{17}\text{O})$  couplings from the GIPAW DFT calculations as the SIMPSON input, hence the reliance on

accurate DFT prediction in this study. The resultant simulated spin-echo dephasing curves produced are in good agreement (within error) with those experimentally derived.

The geometry optimised DFT structure derived using the CASTEP code gives a firm agreement with the experimentally measured shifts observed for the ether ( $\delta_{\text{iso}} = 223$ ,  $P_Q = 9.4$  MHz) and hydroxyl ( $\delta_{\text{iso}} = 62$ ,  $P_Q = 10.5$  MHz) groups, however the unoptimised experimental structure has better agreement for the carbonyl group ( $\delta_{\text{iso}} = 320$ ,  $P_Q = 8.3$  MHz). The determined  $\delta_{\text{iso}}$  and  $\eta_Q$  values for the latter are shown to be consistent with bond lengths closer to 1.222 Å emanating from the unoptimised experimental XRD structure, rather than the geometry optimised length of 1.238 Å. The geometry optimised DFT  $^1J(^{13}\text{C}, ^{17}\text{O})$  coupling to the hydroxyl is calculated as 20 Hz and the  $^1J_{\text{CO}}$  couplings to the ether oxygen were calculated to be 37 (O–C=O) and 32 (O–C–OH) Hz. These measurements are all within error of the experimental echo decays.

## Conflicts of interest

There are no conflicts to declare.

## Acknowledgements

JVH acknowledges support for the solid state NMR instrumentation at Warwick used in this research which was funded by EPSRC (grants EP/M028186/1 and EP/K024418/1) and the University of Warwick, with additional partial funding being provided through the Birmingham Science City Advanced Materials Projects 1 and 2, which were supported by Advantage West Midlands (AWM) and the European Regional Development Fund (ERDF). The UK 850 MHz National Solid State NMR Facility used in this research is also acknowledged; this was funded by the EPSRC, BBSRC and the University of Warwick which included partial funding *via* the Birmingham Science City Advanced Materials Projects 1 and 2, supported by Advantage West Midlands (AWM) and the European Regional Development Fund (ERDF). JVH also acknowledges the University of Warwick Scientific Computing Research Technology Platform (RTP), and EPSRC grant EP/K000128/1, for access to the TINUS and MINERVA high performance computing clusters, respectively, that facilitated the computational effort undertaken in this work. JDW thanks the EPSRC for grant EP/E018203/1 from the Physical Organic Chemistry Initiative, and Nottingham Trent University for financial support.

## References

- 1 J. Clayden, N. Greeves and S. Warren, *Organic Chemistry*, OUP Oxford, 2012.
- 2 S. Mandal, S. Mandal, S. K. Ghosh, P. Sar, A. Ghosh, R. Saha and B. Saha, *RSC Adv.*, 2016, **6**, 69605–69614.
- 3 A. Williamson, *London, Edinburgh Dublin Philos. Mag. J. Sci.*, 1850, **37**, 350–356.





- 4 Z. Wang, *Comprehensive Organic Name Reactions and Reagents*, John Wiley & Sons, Inc., 2010, DOI: 10.1002/9780470638859.conrr480.
- 5 M. T. Scerba, A. F. DeBlase, S. Bloom, T. Dudding, M. A. Johnson and T. Lectka, *J. Phys. Chem. A*, 2012, **116**, 3556–3560.
- 6 S. Lau, B. Ward, X. Zhou, A. J. P. White, I. J. Casely, S. A. Macgregor and M. R. Crimmin, *Organometallics*, 2017, **36**, 3654–3663.
- 7 G. Saritemur, L. Nomen Miralles, D. Husson, M. B. Pitak, S. J. Coles and J. D. Wallis, *CrystEngComm*, 2016, **18**, 948–961.
- 8 A. Choudhary, K. J. Kamer and R. T. Raines, *J. Org. Chem.*, 2011, **76**, 7933–7937.
- 9 K. J. Kamer, A. Choudhary and R. T. Raines, *J. Org. Chem.*, 2013, **78**, 2099–2103.
- 10 A. Choudhary, C. G. Fry, K. J. Kamer and R. T. Raines, *Chem. Commun.*, 2013, **49**, 8166–8168.
- 11 A. Choudhary, R. W. Newberry and R. T. Raines, *Org. Lett.*, 2014, **16**, 3421–3423.
- 12 R. W. Newberry, G. J. Bartlett, B. VanVeller, D. N. Woolfson and R. T. Raines, *Protein Sci.*, 2014, **23**, 284–288.
- 13 G. J. Bartlett, R. W. Newberry, B. VanVeller, R. T. Raines and D. N. Woolfson, *J. Am. Chem. Soc.*, 2013, **135**, 18682–18688.
- 14 H. Kessler, C. Griesinger, J. Lautz, A. Mueller, W. F. Van Gunsteren and H. J. C. Berendsen, *J. Am. Chem. Soc.*, 1988, **110**, 3393–3396.
- 15 M. Karplus, *J. Am. Chem. Soc.*, 1963, **85**, 2870–2871.
- 16 I. Hung, A.-C. Uldry, J. Becker-Baldus, A. L. Webber, A. Wong, M. E. Smith, S. A. Joyce, J. R. Yates, C. J. Pickard, R. Dupree and S. P. Brown, *J. Am. Chem. Soc.*, 2009, **131**, 1820–1834.
- 17 D. H. Barich, J. M. Davis, L. J. Schieber, M. T. Zell and E. J. Munson, *J. Pharm. Sci.*, 2006, **95**, 1586–1594.
- 18 S. Penzel, A. A. Smith, V. Agarwal, A. Hunkeler, M.-L. Org, A. Samoson, A. Böckmann, M. Ernst and B. H. Meier, *J. Biomol. NMR*, 2015, **63**, 165–186.
- 19 K. Sharma, P. K. Madhu and V. Agarwal, *J. Magn. Reson.*, 2016, **270**, 136–141.
- 20 M. Profeta, F. Mauri and C. J. Pickard, *J. Am. Chem. Soc.*, 2003, **125**, 541–548.
- 21 J. Clark Stewart, D. Segall Matthew, J. Pickard Chris, J. Hasnip Phil, I. J. Probert Matt, K. Refson and C. Payne Mike, *Z. Kristallogr.*, 2005, **220**, 567.
- 22 J. R. Yates, C. J. Pickard and F. Mauri, *Phys. Rev. B: Condens. Matter Mater. Phys.*, 2007, **76**, 024401.
- 23 T. F. G. Green and J. R. Yates, *J. Chem. Phys.*, 2014, **140**, 234106.
- 24 A. P. M. Kentgens, W. S. Veeman and J. Van Bree, *Macromolecules*, 1987, **20**, 1234–1237.
- 25 A. G. Stepanov, V. N. Zudin and K. I. Zamaraev, *Solid State Nucl. Magn. Reson.*, 1993, **2**, 89–93.
- 26 D. Massiot, F. Fayon, M. Deschamps, S. Cadars, P. Florian, V. Montouillout, N. Pellerin, J. Hiet, A. Rakhmatullin and C. Bessada, *C. R. Chim.*, 2010, **13**, 117–129.
- 27 A. Lesage, M. Bardet and L. Emsley, *J. Am. Chem. Soc.*, 1999, **121**, 10987–10993.
- 28 A. Lesage, S. Steuernagel and L. Emsley, *J. Am. Chem. Soc.*, 1998, **120**, 7095–7100.
- 29 A. Lesage, C. Auger, S. Caldarelli and L. Emsley, *J. Am. Chem. Soc.*, 1997, **119**, 7867–7868.
- 30 S. P. Brown and L. Emsley, *J. Magn. Reson.*, 2004, **171**, 43–47.
- 31 S. P. Brown, *Solid State Nucl. Magn. Reson.*, 2012, **41**, 1–27.
- 32 R. K. Harris, E. D. Becker, S. M. Cabral de Menezes, R. Goodfellow and P. Granger, *Magn. Reson. Chem.*, 2002, **40**, 489–505.
- 33 R. Dupree, *eMagRes*, John Wiley & Sons, Ltd, 2007, DOI: 10.1002/9780470034590.emrst1203.
- 34 D. Massiot, F. Fayon, M. Capron, I. King, S. Le Calve, B. Alonso, J. O. Durand, B. Bujoli, Z. H. Gan and G. Hoatson, *Magn. Reson. Chem.*, 2002, **40**, 70–76.
- 35 M. Bak, J. T. Rasmussen and N. C. Nielsen, *J. Magn. Reson.*, 2000, **147**, 296–330.
- 36 C. J. Pickard and F. Mauri, *Phys. Rev. B: Condens. Matter Mater. Phys.*, 2001, **63**, 245101.
- 37 S. A. Joyce, J. R. Yates, C. J. Pickard and F. Mauri, *J. Chem. Phys.*, 2007, **127**, 204107.
- 38 G. J. Rees, S. P. Day, A. Lari, A. P. Howes, D. Iuga, M. B. Pitak, S. J. Coles, T. L. Threlfall, M. E. Light, M. E. Smith, D. Quigley, J. D. Wallis and J. V. Hanna, *CrystEngComm*, 2013, **15**, 8823–8839.
- 39 F. H. Allen, O. Kennard, D. G. Watson, L. Brammer, A. G. Orpen and R. Taylor, *J. Chem. Soc., Perkin Trans. 2*, 1987, S1–S19, DOI: 10.1039/P29870000051.
- 40 M. P. Hanrahan, A. Venkatesh, S. L. Carnahan, J. L. Calahan, J. W. Lubach, E. J. Munson and A. J. Rossini, *Phys. Chem. Chem. Phys.*, 2017, **19**, 28153–28162.
- 41 J. K. Williams, K. Schmidt-Rohr and M. Hong, *Solid State Nucl. Magn. Reson.*, 2015, **72**, 118–126.
- 42 T. D. Ferris and T. C. Farrar, *Mol. Phys.*, 2002, **100**, 303–309.
- 43 L. S. Batchelder, J. Clymer and J. L. Ragle, *J. Chem. Phys.*, 1981, **74**, 4791–4799.
- 44 G. Wu, I. Hung, Z. Gan, V. V. Tersikh and X. Kong, *J. Phys. Chem. A*, 2019, **123**, 8243–8253.
- 45 M. Bak, J. T. Rasmussen and N. C. Nielsen, *J. Magn. Reson.*, 2011, **213**, 366–400.
- 46 V. Lemaître, M. E. Smith and A. Watts, *Solid State Nucl. Magn. Reson.*, 2004, **26**, 215–235.
- 47 X. Kong, Y. Dai and G. Wu, *Solid State Nucl. Magn. Reson.*, 2017, **84**, 59–64.
- 48 K. J. Pike, V. Lemaître, A. Kukol, T. Anupöld, A. Samoson, A. P. Howes, A. Watts, M. E. Smith and R. Dupree, *J. Phys. Chem. B*, 2004, **108**, 9256–9263.
- 49 X. Kong, V. V. Tersikh, R. L. Khade, L. Yang, A. Rorick, Y. Zhang, P. He, Y. Huang and G. Wu, *Angew. Chem., Int. Ed.*, 2015, **54**, 4753–4757.
- 50 K. Yamauchi, S. Kuroki and I. Ando, *J. Mol. Struct.*, 2002, **602–603**, 171–175.
- 51 K. Yamauchi, S. Kuroki, I. Ando, T. Ozaki and A. Shoji, *Chem. Phys. Lett.*, 1999, **302**, 331–336.
- 52 C. Gervais, R. Dupree, K. J. Pike, C. Bonhomme, M. Profeta, C. J. Pickard and F. Mauri, *J. Phys. Chem. A*, 2005, **109**, 6960–6969.
- 53 K. J. D. MacKenzie and M. E. Smith, *Multinuclear Solid-State Nuclear Magnetic Resonance of Inorganic Materials*, Pergamon Press, Oxford, 2002.



- 54 A. Samoson and E. Lippmaa, *J. Magn. Reson.*, 1989, **84**, 410–416.
- 55 A. Samoson, *Chem. Phys. Lett.*, 1985, **119**, 29–32.
- 56 B. P. de Laune, G. J. Rees, J. F. Marco, H.-Y. Hah, C. E. Johnson, J. A. Johnson, F. J. Berry, J. V. Hanna and C. Greaves, *Inorg. Chem.*, 2017, **56**, 10078–10089.
- 57 J. V. Hanna, K. J. Pike, T. Charpentier, T. F. Kemp, M. E. Smith, B. E. G. Lucier, R. W. Schurko and L. S. Cahill, *Chem. – Eur. J.*, 2010, **16**, 3222–3239.
- 58 C. S. Griffith, V. Luca, J. V. Hanna, K. J. Pike, M. E. Smith and G. S. Thorogood, *Inorg. Chem.*, 2009, **48**, 5648–5662.
- 59 C. Jager, *NMR Basic Principles and Progress*, Springer Verlag, Berlin, 1994, p. 135.
- 60 A. Wong, I. Hung, A. P. Howes, T. Anupöld, J. Past, A. Samoson, S. P. Brown, M. E. Smith and R. Dupree, *Magn. Reson. Chem.*, 2007, **45**, S68–S72.
- 61 A. Wong, A. P. Howes, K. J. Pike, V. Lemaître, A. Watts, T. Anupöld, J. Past, A. Samoson, R. Dupree and M. E. Smith, *J. Am. Chem. Soc.*, 2006, **128**, 7744–7745.
- 62 X. Kong, A. Brinkmann, V. Tersikh, R. E. Wasylishen, G. M. Bernard, Z. Duan, Q. Wu and G. Wu, *J. Phys. Chem. B*, 2016, **120**, 11692–11704.
- 63 J. Lu, I. Hung, A. Brinkmann, Z. Gan, X. Kong and G. Wu, *Angew. Chem., Int. Ed.*, 2017, **56**, 6166–6170.
- 64 L. Duma, W. C. Lai, M. Carravetta, L. Emsley, S. P. Brown and M. H. Levitt, *ChemPhysChem*, 2004, **5**, 815–833.
- 65 F. A. Perras and D. L. Bryce, *J. Magn. Reson.*, 2014, **242**, 23–32.
- 66 M. Karplus, *J. Chem. Phys.*, 1959, **30**, 11–15.
- 67 B. Wrackmeyer, *Z. Naturforsch., B: J. Chem. Sci.*, 2004, **59**, 286–290.
- 68 R. E. Wasylishen, J. O. Friedrich, S. Mooibroek and J. B. Macdonald, *J. Chem. Phys.*, 1985, **83**, 548–551.

